Investigating the Effectiveness of Supervised and Unsupervised Classification for Landsat Images Utilizing Classification Accuracy Assessment.

Hayder Hameed Jassoom [1,*], Rabab Saadoon Abdoon [2]

[1,2] Department of Physics, Collage of Science, University of Babylon, Babil, Iraq.
*Corresponding author : ✉: sci685.hadiar.hamied@student.uobabylon.edu.iq.

Article Information

Abstract

This study filled in gaps in 2012 Landsat-7 satellite images using the "Nearest Similar Pixel Processor" algorithm. Changes in LU/LC coverage in Babil province were classified and tracked during the period from 1999 to 2023. Landsat-7 and Landsat-8 satellite images were relied upon, focusing on specific spectral bands that provide a spatial resolution of 30 meters. Two classification methods were utilized: Maximum Likelihood for supervised classification and ISO Data for unsupervised classification. A metric of precision was employed to assess the effectiveness of individual classification techniques. This metric is determined by the ratio of correctly classified data points to the overall dataset size. The research conducted a comparative analysis of land use/land cover classification methodologies utilizing Landsat imagery: maximum likelihood classification and unsupervised ISO Cluster classification. The findings indicated that the MLC approach outperformed the ISO Cluster method in terms of accuracy. Four distinct land use coverage categories have been identified: urban, bare soil, water bodies, and vegetated lands. The study revealed significant changes in all land use coverage categories within Babil province from 1999 to 2023. In particular, the urban land area showed a significant increase, while the arid land area showed a decrease. The area of water bodies varied during the study period, most likely due to differences in water discharge from the Euphrates River, which is affected by agreements between Iraq and Turkey and changes in rainfall. The distribution of vegetation covers also showed annual differences due to the relevant authorities' marketing plan for growing agricultural crops.

1. Introduction:

The identification of Land Use/Land Cover (LU/LC) features has become a fundamental component in various Geographic Information Technology (GIT) applications [1], [2]. LU/LC change analysis is an essential tool for landscape transformation detection, as technological advances have greatly improved LU/LC analysis techniques, enhancing the accu-

racy and efficiency of change detection [3], [4]. Land cover data is a valuable tool for monitoring and tracking urban and industrial developments and natural resource conservation. By analyzing this data, one can understand land use changes, identify vulnerable areas, and assess the effectiveness of sustainable development plans [5], [6], [7], [8].

Remote sensing data provides a rich source of information about the Earth's surface. However, this data is raw images that cannot be understood unless processed and analyzed [9], [10]. Over the past few years, numerous techniques for classifying images from remotely sensed data have been developed. Ground surveying has increased in recent years, resulting in a corresponding increase in data volumes; this has accelerated

the rate of remote sensing over the past few years [11], [12]. Classification of land use and land cover provides nations with the knowledge to make well-informed decisions utilizing remote sensing data. Understanding and identifying land change is critical in conserving, managing, and planning for development. Knowledge of the changes in environmental dynamics is also beneficial for formulating policies that maximize these lands' use and ensure sustainable development. The classification of land use and land cover is essential for determining the relationship between human activity and the environment [13]. In image classification, there are two types of techniques: learning and unsupervised learning.

Table 1. Landsat Image Information.

Path	Row	Landsat 7 (+ETM)		Landsat 8 (OLI/TRIS)
168	37	12 / July / 1999	15 / July / 2012	22 / July / 2023
168	38	12 / July / 1999	15 / July / 2012	22 / July / 2023
169	37			29/ July / 2023

1.1 Supervised Learning:

Supervised classification techniques entail the analyst's responsibility of selecting the training areas in order to ascertain the properties and characteristics of each category. The extraction of discriminating information is utilized to categorize every pixel in the image [14]. Supervised learning is more effective when the user specifies measurable outcomes that the data samples should reflect. In supervised learning, the analyst assumes a critical function by identifying training sites that serve as representations of the spectral attributes of recognized regions. These sites are then utilized to train the classifier. The training data is defined by the analyst to closely resemble the classes and features that are utilized in the classifier's analysis. The characteristics of each class are derived from the training data that has been extracted. Supervised classification is executed in two distinct phases: training and assessment.

The training phase consists of training the classifier, while the testing phase evaluates the performance of the classifier on unknown pixels. The analyst is responsible for designating regions during the training phase; these regions are subsequently utilized to extract information from the training data. This data facilitates the estimation of the properties of the data involved in the classification assignment [15], [16]. The labelling of unclear pixels occurs subsequent to the classification stage, utilizing their spectral similarity in the training data. Pixels lacking spectral similarity with any previously identified class are allocated an unidentified class. Each pixel of the resulting image is assigned a class designation. The efficacy of the classifier is predominantly contingent upon the attributes of the training data, which were determined in consultation with the analyst [14].

1.2 Unsupervised Learning

Unsupervised classification is a method that utilizes the evaluation of pixel-relative positions to identify clusters within the input data. It is supposed that each cluster corresponds to distinct characteristics. These clusters are generated through the utilization of the reflectance property of pixels [15]. Specifying the number of clusters to be generated and the bands to be selected is the responsibility of the user. The software utilized for image classification generates clusters on the basis of this data. The user performs manual class identification in accordance with the formed classes. When multiple classes correspond to the same class, the user is responsible for merging those classes.

Therefore, unsupervised learning is highly applicable in situations where the user is unaware of the specific subdivisions that should be applied to the data samples. Unsupervised learning is employed in such circumstances to produce distinct classes, which are alternatively referred to as spectrally inseparable classes or clusters. In order to acquire these clusters, the variance is computed both between and within the clusters [17], [18].

Accuracy assessment of land use and land cover classification was conducted using Kappa coefficient and confusion matrix. Confusion matrix is a common tool to evaluate the accuracy of land use and land cover classification methods. Analyzing the confusion matrix is very effective for assessing the accuracy of land use and land cover classification. It is used to calculate the classification performance and identify the number of true positives and negatives, false positives and false negatives, which provides deeper insights into the classification process. The overall accuracy is calculated as follows:

$$Overall\ accuracy = \frac{D}{N} \times 100\% \qquad (1)$$

Where D represents the total number of correct calls as summed along the major diagonal, and N represents the total number of correct calls in the error matrix. While the kappa coefficient is calculated as follows:

$$\hat{k} = \frac{N\sum_{i=1}^{r} X_{ii} - \sum_{i=1}^{r} X_{i+} \times X_{+i}}{N^2 - \sum_{i=1}^{r} X_{i+} \times X_{+i}} \qquad (2)$$

Where N represent total number of cells in the error matrix, r represents number of row in matrix, X_{ii} represents total number correct cells in a class (i.e. value in row i and column i), X_{i+} represents total for row i , X_{+i} represents total for column i.

This study aims to determine the optimal algorithm for classifying Landsat-7 (+ETM) and Landsat-8 (OLI) data that

Table 2. Confusion Matrix for Maximum Likelihood Classifier in 1999.

ID	Classes	Urban lands	Bare soil lands	Water bodies	Vegetation lands	Row total	User accuracy	Kappa
1	Urban lands	40	2	0	2	44	0.909091	0
2	Bare soil lands	2	121	0	8	131	0.923664	0
3	Water bodies	0	1	9	0	10	0.9	0
4	Vegetation lands	0	6	0	67	73	0.917808	0
5	Column total	42	130	9	77	258	0	0
6	Producer accuracy	0.952381	0.930769	1	0.87013	0	0.918605	0
7	Kappa	0	0	0	0	0	0	0.870923

Table 3. Confusion Matrix for Maximum Likelihood Classifier in 2012.

ID	Classes	Urban lands	Bare soil lands	Water bodies	Vegetation lands	Row total	User accuracy	Kappa
1	Urban lands	37	5	0	0	42	0.880952	0
2	Bare soil lands	1	99	0	4	104	0.951923	0
3	Water bodies	0	0	9	1	10	0.9	0
4	Vegetation lands	0	5	0	96	101	0.950495	0
5	Column total	38	109	9	101	257	0	0
6	Producer accuracy	0.973684	0.908257	1	0.950495	0	0.937743	0
7	Kappa	0	0	0	0	0	0	0.903984

are available in ArcMap 10.8. The maximum likelihood classifier and the ISO cluster were compared because ArcMap 10.8 software only offered a limited number of classification methods. The best of these methods was then utilized to identify changes in the LULC area of the Babil province for the period 1999–2023.

2. Study Area:

The province of Babil situates in the center of Iraq. It is surrounded by five provinces: Baghdad province borders it to the north, Wassit province to the east, Holy Karbala and Al-Anbar provinces to the west, Al-Najaf Al-Ashraf and Al-Qadisiyah provinces to the south. It is situated latitudinally between 43° 58' 10" and 44° 38' 35" east of Greenwich and north of the equator between 32° 7' 25" and 33° 0' 35". The Babil province has an area of about 5335 km2 with a population of approximately 2,065,042, according to the 2018 population census. The Babil province consists of five administrative regions: Al-Hillah, Al-Muhawwil, Al-Musayyib, Al-Hashimiya, and Al-Hamza Al-Gharbi. Babil province has an arid climate, with summertime temperatures surpassing 40 degrees Celsius. Between April and November, precipitation is scarce, averaging 100 mm annually. Agriculture holds significant economic value in Babil province due to the region's substantial production of cereals, vegetables, and fruits. Many plantations and orchards in Babil province are watered by an extensive network of canals [19]. Emphasizing the province's

borders, Figure 1 illustrates the geographic location of Babil province.

3. Methodology:

3.1 Approved method:

Figure 1 shows the standard procedure for converting raw remote sensing data into classified data through the use of two different classification algorithms.

3.2 Landsat Data:

The collected data are from various sources, including Landsat satellite images for 1999, 2012, and 2023, downloaded from the United States Geological Survey website [20]. These images were characterized by their clarity and lack of clouds, as shown in Table 1. The shapefile of Iraq's administrative boundaries was also obtained from the Office of the Coordination of Humanitarian Affairs of the United Nations [21].

3.3 Radiometric Calibration:

Radiometric calibration is a fundamental and critical step in converting remote sensing information into quantifiable values [22]. In this work, the Radiometric calibration was performed using ENVI 5.6 software to achieve the study's objectives.
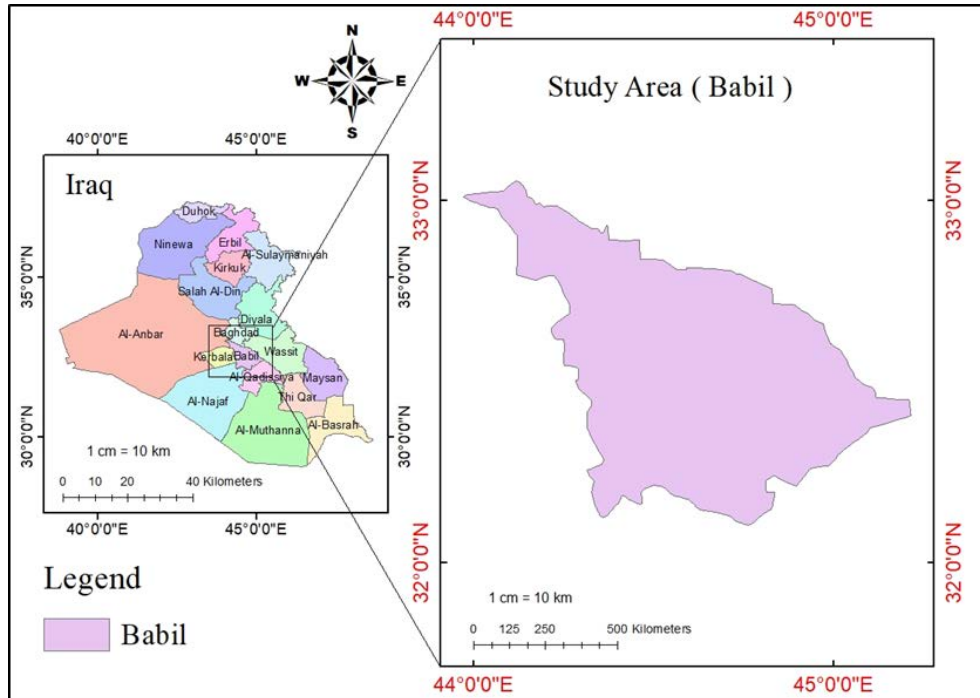
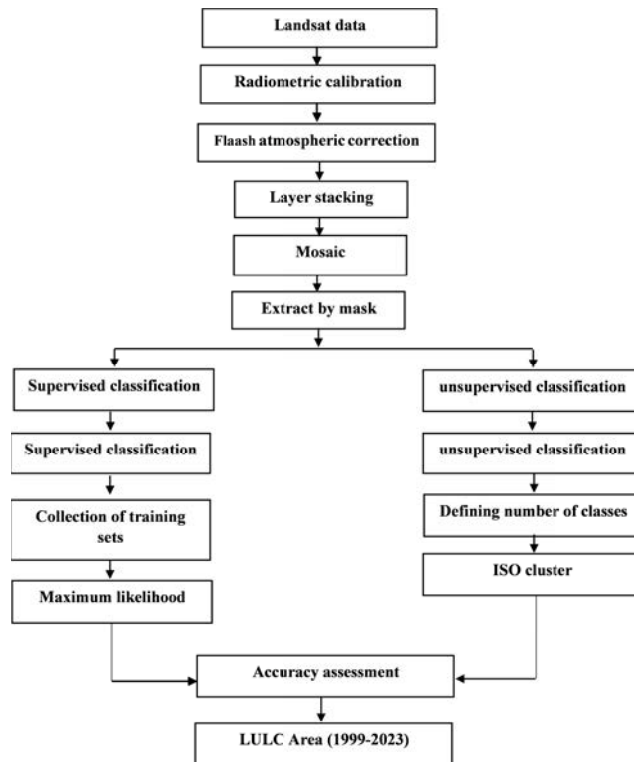**Figure 1.** The geographical location of Babil province.

Figure 2. Diagram of the adopted procedures.

Table 4. Confusion Matrix for Maximum Likelihood Classifier in 2023.

ID	Classes	Urban lands	Bare soil lands	Water bodies	Vegetation lands	Row total	User accuracy	Kappa
1	Urban lands	56	10	0	1	67	0.835821	0
2	Bare soil lands	3	91	0	1	95	0.957895	0
3	Water bodies	0	0	9	1	10	0.9	0
4	Vegetation lands	0	9	0	71	80	0.8875	0
5	Column total	59	110	9	74	252	0	0
6	Producer accuracy	0.949153	0.827273	1	0.959459	0	0.900794	0
7	Kappa	0	0	0	0	0	0	0.853798

Table 5. Confusion matrix for ISO Cluster unsupervised classification in 1999.

ID	Classes	Urban lands	Bare soil lands	Water bodies	Vegetation lands	Row total	User accuracy	Kappa
1	Water bodies	21	20	2	0	43	0.488372	0
2	Vegetation lands	18	63	8	5	94	0.670213	0
3	Urban lands	0	0	46	33	79	0.582278	0
4	Bare soil lands	0	2	9	23	34	0.676471	0
5	Column total	39	85	65	61	250	0	0
6	Product accuracy	0.538462	0.741176	0.707692	0.377049	0	0.612	0
7	Kappa	0	0	0	0	0	0	0.468482

3.4 Atmospheric Correction:

Atmospheric correction plays a vital role in many applications that rely on image analysis, especially those that require accurate measurements of Earth's surface properties. In these applications, small variations in the reflectance of the Earth's surface can lead to inaccurate results, making atmospheric correction essential for obtaining reliable information [23]. ENVI 5.6 software was used to correct atmospheric effects in the images of this work.

3.5 Gap fill:

On May 31, 2003, the scan line corrector of the ETM+ sensor on the Landsat 7 satellite failed. As a result, wedge-shaped gaps appeared in the images, ranging in width from one pixel near the center of the image to about 12 pixels towards the edges of the scene. These gaps constitute approximately 22% of the pixels in the image. [24], these gaps were processed for Landsat 7 images for the year 2012, using the "nearest similar pixel processor" or the NSPI algorithm. This algorithm assumes that neighboring pixels of the same class, such as land cover, have similar spectral characteristics. Therefore, the values of neighboring pixels can be used to estimate the value of the missing pixel. [25]. The objective of the study was achieved, and the missing data was restored using ENVI 5.6 software, using the "Single Gap Fill (Triangulation)" tool after performing radiometric correction (radiometric calibration and atmospheric correction).

3.6 Layer Stacking:

Raw remote sensing data typically comprises multiple spectral bands, each with a different spatial resolution. The spatial resolution of each band defines the smallest ground distance represented by an individual pixel in the remote-sensing image. Lower spatial resolution values correspond to higher overall data accuracy. Since the Landsat 7 data in Table 1 consists of 8 bands with varying spatial resolutions, bands 1, 2, 3, 4, 5, and 7 were merged to have consistent resolution. While Landsat 8 data in Table 2 consists of 11 bands with varying spatial resolutions, spectral bands 1, 2, 3, 4, 5, 6, and 7 were merged to have consistent resolution. This ensures consistent accuracy across all data, making it more useful for analysis. Image processing techniques like composite bands allow the integration of different image derivatives while maintaining consistent spatial detail (30 meters). This creates highly accurate output images suitable for advanced classification tasks.

3.7 Mosaic:

Image fusion is an advanced technique used to combine two or more images with an overlapping area so that the coordinates become identical. The inputs (images to be merged) must have the same number of bands and pixel depth. This technique merged two satellite images from Landsat 7 (+ETM) for the years 1999 and 2012 and three from Landsat 8 (OLI) for the year 2023. Then, specific areas of interest are extracted

Table 6. Confusion matrix for ISO Cluster unsupervised classification in 2012.

ID	Classes	Urban lands	Bare soil lands	Water bodies	Vegetation lands	Row total	User accuracy	Kappa
1	Water bodies	21	15	1	0	37	0.567568	0
2	Vegetation lands	16	59	7	3	85	0.694118	0
3	Urban lands	0	0	40	43	83	0.481928	0
4	Bare soil lands	0	3	17	25	45	0.555556	0
5	Column total	37	77	65	71	250	0	0
6	Product accuracy	0.567568	0.766234	0.615385	0.352113	0	0.58	0
7	Kappa	0	0	0	0	0	0	0.429298

Table 7. Confusion matrix for ISO Cluster unsupervised classification in 2023.

ID	Classes	Urban lands	Bare soil lands	Water bodies	Vegetation lands	Row total	User accuracy	Kappa
1	Water bodies	19	21	0	0	40	0.475	0
2	Vegetation lands	17	44	5	7	73	0.60274	0
3	Urban lands	0	0	41	36	77	0.532468	0
4	Bare soil lands	0	5	34	22	61	0.360656	0
5	Column total	36	70	80	65	251	0	0
6	Product accuracy	0.527778	0.628571	0.5125	0.338462	0	0.501992	0
7	Kappa	0	0	0	0	0	0	0.322735

using the "Extract by Mask" tool, removing unnecessary background data. This allows for more accurate image analysis.

3.8 Classification Algorithms:

The following classification algorithms were applied to raster data:

Firstly, Supervised Classification:

Image classification techniques that rely on remote sensing data are now used in various applications [26]. A set of training data called "representative training samples" for each class of remote sensing images (false color composite) is used to obtain results through supervised classification algorithms. Training samples are known identity areas, also called the region of interest [27].

• The Maximum Likelihood Classifier assigns a pixel to the class with the highest probability of containing that pixel based on the statistical characteristics of the class. Users can define a threshold to exclude pixels with probabilities below a certain level, resulting in unclassified pixels. In order to designate training areas, one or more polygons were selected for every class. Pixels that are contained within the training area are designated as the training pixels for a specific class. When determining an appropriate training area for a specific class, two crucial attributes are considered: the area's uniformity and the degree to which it accurately represents the same class across the entire image [28].

Secondly, Unsupervised Classification: Unlike supervised learning, unsupervised classification doesn't need pre-labeled data for training. Instead, the user specifies the desired number of classes and the number of processing steps to identify natural groupings within the data.

• The ISO cluster unsupervised classification employs an iterative process to group pixels based on their spectral characteristics. Pixels with similar spectral signatures are grouped, while a user-defined distance threshold determines cluster separation. This method requires the user to specify the desired number of classes and the number of processing steps beforehand [27].

3.9 Accuracy Assessment:

Accuracy assessment is estimated and compared using the applied classification results. Accuracy assessment is determined using the true ground reference area that was collected.

4. Results and Discussion:

4.1 The results of the classification:

The outcomes of applying supervised and unsupervised classification to Landsat-7 (+ETM) and Landsat 8 (OLI) data are depicted in Figure 3(a, b, c), Figure 5(a, b, c) and Figure **??**(a, b, c). The data was classified into four classes: urban areas, bare soil, water bodies, and Vegetation lands. In supervised classification, 25 samples were collected from each

Table 8. Detailed description of classes.

NO.	Classes	Description
1	Urban lands	Land that is covered with buildings
2	bare soil lands	refers to territory devoid of vegetation, land use, and agricultural activities
3	Water bodies	consist of lakes, rivers, and irrigation canals.
4	Vegetation lands	comprises agricultural produce, public parks, and orchards.
5	Other lands	

Table 9. Land use / land cover changes in Babil province between 1999 and 2023.

Classes	Years/Area (km2)		
	1999	2012	2023
Urban lands	1124.26	1467.69	1729.84
bare soil lands	2848.73	2082.00	1982.65
Water bodies	68.30	163.10	61.10
Vegetation lands	1294.16	1622.51	1561.69
Other lands	0.19	0.34	0.36
Total	5335.64	5335.64	5335.64

class to ascertain the training sets. The larger the classes, the better the pixel clustering, so the number of samples was set to a maximum. The samples collected were smaller elliptical segments and were distributed to cover all areas of the feature. The maximum likelihood classification results were best, and land use/land cover features were accurately identified. The results exhibited the most remarkable resemblance to the original remote-sensing images. At the same time, the images classified by ISO Cluster unsupervised classification have misclassified pixels due to the similarity of pixels between two different classes. It can be observed that the urban area was misclassified as a type of soil, and some types of vegetation were misclassified as water. The ISO Cluster classification results showed lower accuracy than the Maximum Likelihood classification.

4.2 Confusion Matrix:

The confusion matrix serves as a visual representation of how well the classified data matches the reference data. It allows us to calculate two key metrics: overall accuracy and the Kappa coefficient. Overall accuracy, expressed as a percentage, is simply the number of correctly classified locations divided by the total number of reference locations. The Kappa coefficient, ranging from -1 to 1, provides a more robust assessment of agreement between the classified and reference

data, considering the possibility of random agreement. The results of the confusion matrix are described in Tables 2, 3, 4, 5, 6, 7.

4.3 Land Use/Land Cover Change in Babil Province:

Four categories of land were identified: urban lands with bare soil, water bodies, and vegetable lands. Details of the categories are shown in Figure 3 (b), Figure 5 (b), Figure **??** (b), Table 8, and Table 9. There were changes in all land categories in Babel Province. The urban land area increased from 1124.26 km2 in 1999 to 1729.84 km^2 in 2023. The area of barren lands decreased, decreasing from 2848.73 km^2 in 1999 to 1982.65 km2 in 2023. Water bodies witnessed fluctuations between increases and decreases. This is due to the rate of water release from the Euphrates River, which depends on water policies between Iraq and Turkey and changes in average rainfall. The distribution of vegetation in the study area varies every year. Plants are limited to orchards, public gardens, and agricultural plantings. The change in land use and land cover in Babil province for the period from 1999 to 2023 is also presented in Table 10.
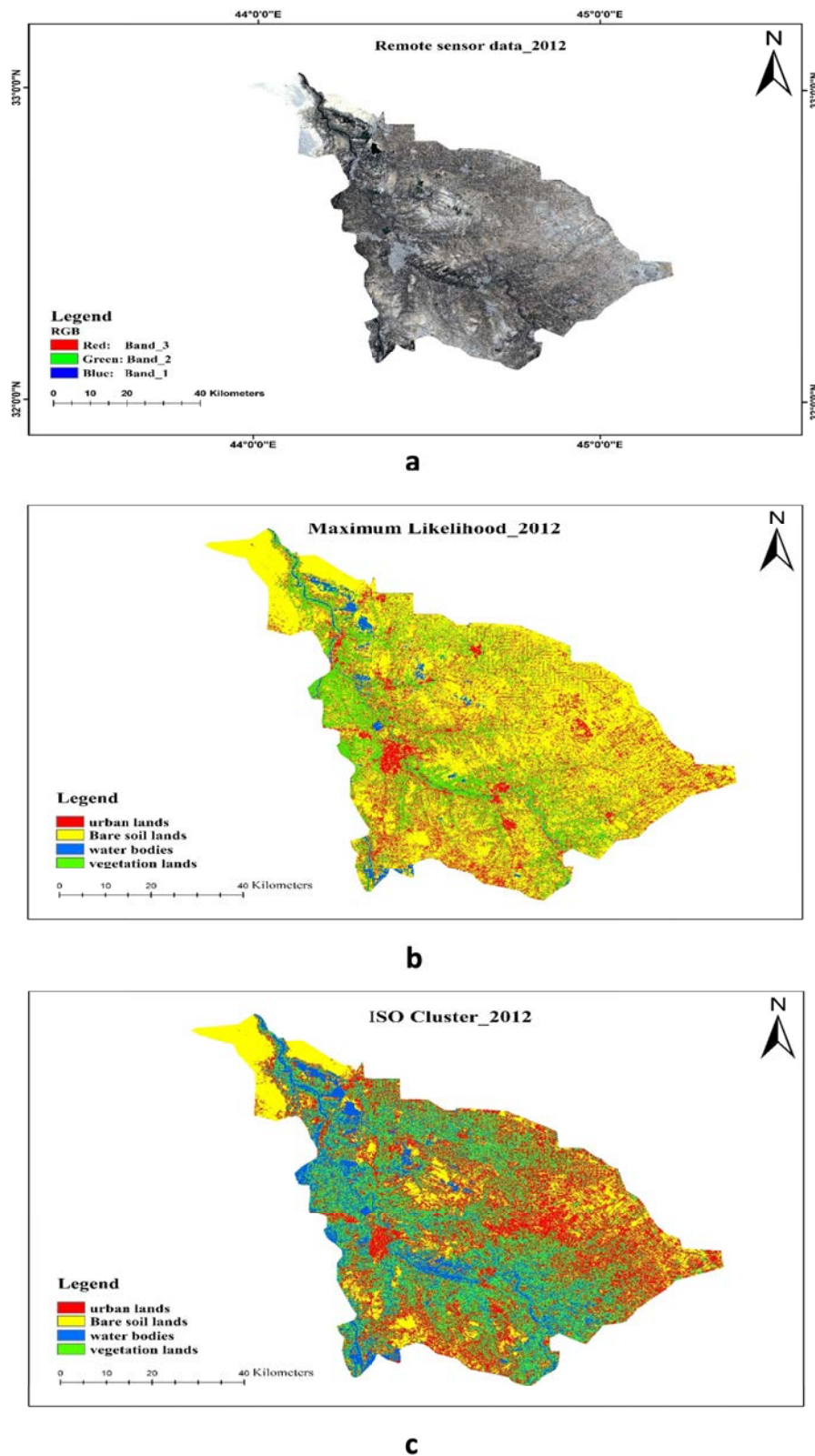
5. Conclusion:

Land use/land cover mapping is a crucial foundation for many spatial applications, demanding high accuracy for sub-
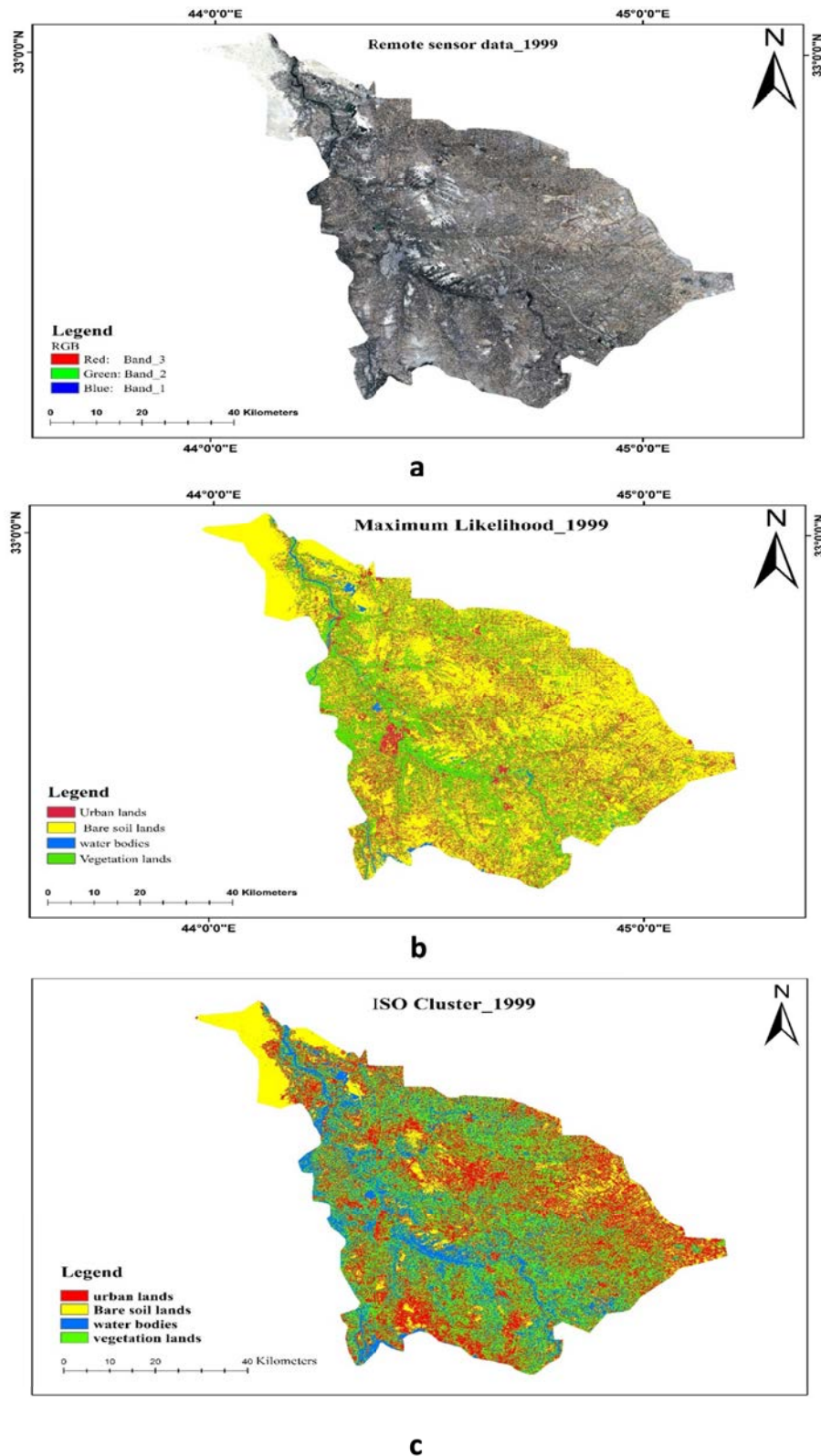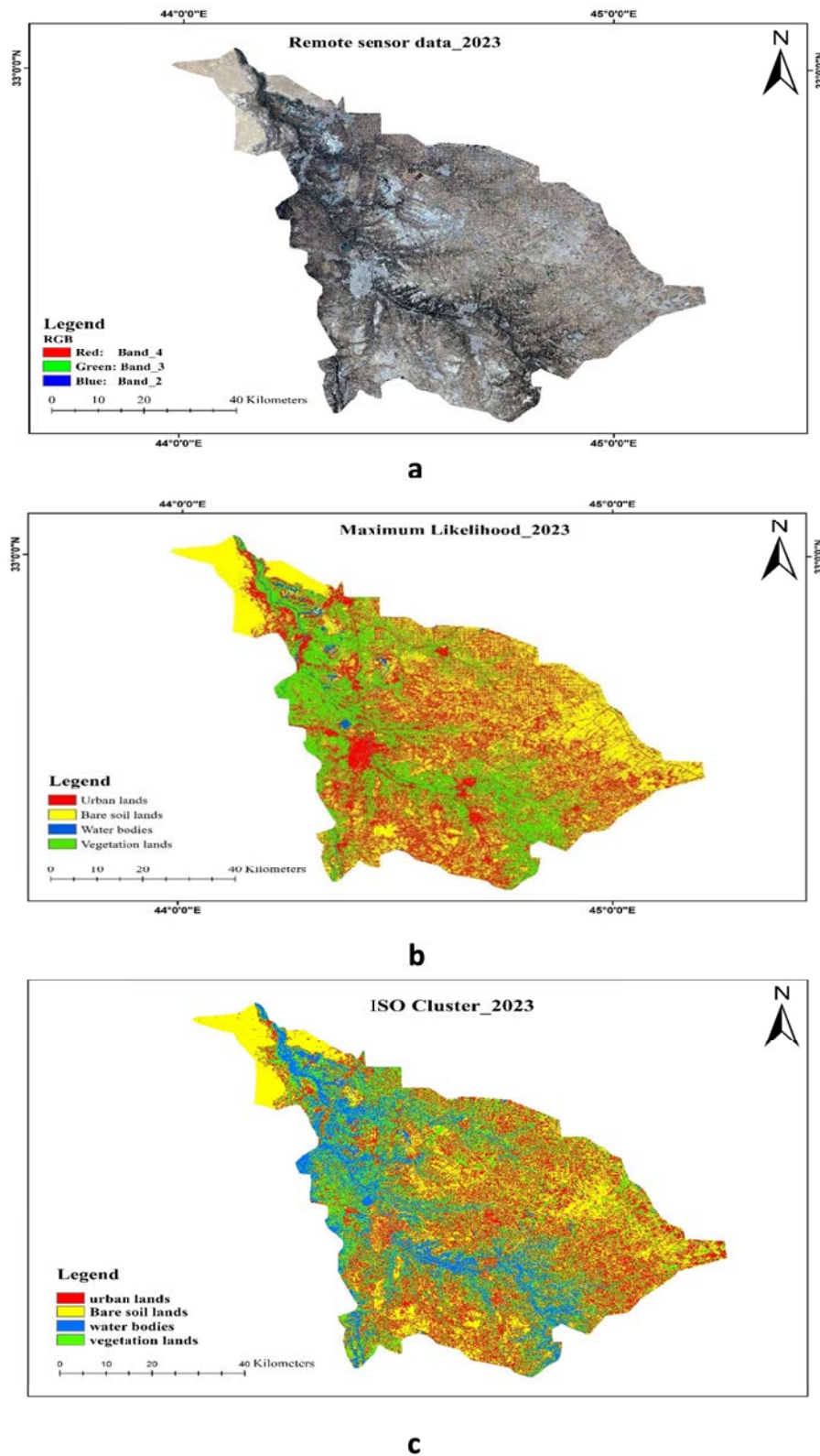
Figure 3. Comparison of classification results for year 1999.
a) Remote sensor data for year 1999.
b) Maximum Likelihood classifier results for year 1999.
c) ISO Cluster unsupervised classification results for year 1999.

Figure 4. Comparison of classification results for year 2012.
a) Remote sensor data for year 2012.
b) Maximum Likelihood classifier results for year 2012.
c) ISO Cluster unsupervised classification results for year 2012.

Figure 5. Comparison of classification results for year 2023.
a) Remote sensor data for year 2023.
b) Maximum Likelihood classifier results for year 2023.
c) ISO Cluster unsupervised classification results for year 2023.

Table 10. Land use / land cover changes trends in Babil province.

Classes	1999		2023		LU/LC change (1999–2023) %
	Area (km^2)	%	Area (km^2)	%	
Urban lands	1124.26	21.07	1729.84	32.42	11.35
bare soil lands	2848.73	53.39	1982.65	37.16	-16.23
Water bodies	68.30	1.28	61.10	1.15	-0.13
Vegetation lands	1294.16	24.26	1561.69	29.27	5.01
Other lands	0.19	0.00	0.36	0.01	0.01
Total	5335.64	100.00	5335.64	100.00	0.00

sequent analyses. Conventional manual digitization methods offer reliable results, and automated classification approaches provide superior accuracy and improved estimation. From the result of this study, it could be concluded that the Maximum Likelihood Classifier successfully interprets land use/land cover features, achieving a total accuracy of 91.86%, 90.01%, and 93.77% for the years 1999,2012, and 2023, respectively. In contrast, the ISO Cluster Data Classifier yielded significantly lower accuracy, with 46.8482%, 42.9298%, and 32.2735% for the years 1999,2012, and 2023, respectively. This compelling evidence suggests the Maximum Likelihood Classifier within the supervised classification framework is the most effective algorithm for classifying land use/land cover features. There are many prospective applications for the methodology across various domains, such as urban planning, agricultural administration, and biodiversity conservation. Land coverage maps and precise land use classification serve practical purposes in urban planning by facilitating the identification of feasible development locations, enabling the estimation of population density, and allowing for the monitoring of alterations to the built environment. The application of these maps in agricultural management enables the identification of land use categories and the estimation of agricultural production, thereby facilitating resource allocation and land use decisions. By identifying regions of significant ecological value and potential threats to biodiversity, the method aids in the formulation of conservation strategies aimed at safeguarding biodiversity. This study strengthens the continuous endeavors to monitor and comprehend alterations in land use and land cover in Babil Province. The acquisition of information is of the utmost importance, as it empowers academia, land managers, and decision-makers to formulate practical approaches that encourage sustainable land use practices and preserve natural resources.

Funding: None.

Data Availability Statement: All of the data supporting the findings of the presented study are available from corresponding author on request.

Declarations:

Conflict of interest: The authors declare that they have no conflict of interest.

Ethical approval: The manuscript has not been published or submitted to another journal, nor is it under review.

References

[1] A. Aqrawi. The nature and preservation of organic matter in holocene lacustrine/deltaic sediments of lower mesopotamia, SE Iraq. *Journal of Petroleum Geology*, 20: 69–90, 1997, doi:10.1111/j.1747-5457.1997.tb00756.x.

[2] C. Baeteman, L. Dupin, and V–M Heyvaert. The persian gulf shorelines and the karkheh, karun, and jarrahi rivers: A geo-archaeological approach. *Geo-Environmental Investigation*, 2: 5–12, 2005.

[3] P. Sanlaville. The deltaic complex of the lower mesopotamian plain and its evolution through millennia, 2002.

[4] A. Aqrawi and G. Evans. Sedimentation in lakes and marshes (ahwar) of the tigris-euphrates delta, southern mesopotamia. *Journal of Sedimentology*, 41: 755–776, 1994, doi:10.1111/j.1365-3091.1994.tb01422.x.

[5] R.G.S. Hudson, F.E. Eames, and G.L. Wilkins. The fauna of some recent marine deposits near basrah. *Iraqi Geological Magazine*, 94(5): 393–401, 1957.

[6] W.A. Macfadyen and C. Vita-Finzi. Mesopotamia: the tigris-euphrates delta and its holocene hammar fauna. *Geological Magazine*, 115(4): 287–300, 1978.

[7] B. Moghaddasi, S. Nabavi, G. Vosoughi, S.M.R Fatemi, and S. Jamili. Abundance and distribution of benthic

foraminifera in the northern oman sea (iranian side) continental shelf sediments. *Research Journal of Environmental Sciences, Academic Journals Inc.*, 2: 210–217, 2009.

[8] V.M.P. Bouchet, E. Alve, B. Rygg, and J. Richard. Benthic foraminifera provide a promising tool for ecological quality assessment of marine waters. *Telford Ecological Indicators*, 23: 66–75, 2012, doi:10.1016/j.ecolind.2012.03.011.

[9] H. Scholz and M. Glaubrecht. Shell and operculum taphonomy of the bithyniid gastropod gabbiella in the pleistocene turkana basin, north kenya. *Journal of Paleontology*, 87(1): 84–90, 2013.

[10] S. Al Sheikhly. Maymouna formation: A new fresh-brackish water formation of quaternary age in southern iraq. *Iraqi Journal of Science*, 42C(4): 120–127, 2001.

[11] R.L. Folk. *Petrology of Sedimentary Rocks*. Hemphill Publishing Company, Austin, 4th edition, 1980.

[12] A.R. Loeblich and H. Tappan. *Foraminiferal Genera and Their Classification*. Van Nostrand Reinhold Company, New Yourk, 1st edition, 1988.

[13] F. Sgarrella and M. Moncharmont Zei. Benthic foraminifera in the gulf of naples (italy): systematics and autoecology. *Bollettino della Societá Paleontologica Italiana*, 32(2): 145–264, 1993.

[14] Y. Lei and T. Li. Ammonia aomoriensis (asano, 1951) and ammonia beccarii (linnaeus, 1758) (foraminifera): Comparisons on their taxonomy and ecological distributions correlated to temperature, salinity and depth. *Acta Micropalaeontologica Sinica*, 32(1): 1–19, 2015.

[15] A.G. Checa and A.P. Jiménez-Jiménez. Constructional morphology, origin, and evolution of the gastropod operculum. *Paleobiology*, 24: 109–132, 1998.

[16] F.W. Welter-Schultes. *European Non-Marine Molluscs, a Guide for Species Identification*. Planet Poster Editions, Göttingen, Germany, 1st edition, 2012.

[17] R. Bhattacharya, N. Das Chatterjee, and G. Dolui. Grain size characterization of instream sand deposition in controlled environment in river kangsabati, west bengal. *Modeling Earth Systems and Environment*, 2(118): 1–14, 2016, doi:10.1007/s40808-016-0173-z.

[18] H.F.L Williams. *Sea-Level Change and delta growth: Fraser Delta, British Columbia*. PhD thesis, Simon Fraser University, Burnaby, British Columbia, 1988.

[19] A. Aqrawi. Stratigraphic signatures of climatic change during the holocene evolution of tigris-euphrates delta, lower mesopotamia. *Journal of Global and Planetary Change*, 28: 267–283, 2001, doi:10.1016/S0921-8181(00)00078-3.

[20] B.M Issa. Depositional environment and biofacies of selected sediments north basra. *Journal of Basrah Research*, 32(5): 1–13, 2010.

[21] G. Bartlett. *Distribution and abundance of foraminifera and thecamoebina in Miramichi River and Bay*. Canada, Bedford Institute of Oceanography, Dartmouth, 1966.

[22] S. Yasufy, K. Watanabe, Y. Kamoi, and I. Kobayashi. Holocene foraminiferal fauna and sedimentary environment in the shirone area, echigo plain, central japan. *Science reports of Niigata University, Series E, (Geology)*, 15: 67–89, 2000.

[23] B.W. Hayward, F. Le Coze, D. Vachard, and O. Gross. *World Foraminifera Database. Quinqueloculina parvula Schlumberger, 1894*. 2021.

[24] A. Goineau, C. Fontanier, M. Mojtahid, A-S. Fanget, M-A. Bassetti, S. Berne, and F. Jorissen. Live–dead comparison of benthic foraminiferal faunas from the rhône prodelta (gulf of lions, nw mediterranean): Development of a proxy for palaeoenvironmental reconstructions. *Marine Micropaleontology*, 119: 17–33, 2015, doi:10.1016/j.marmicro.2015.07.002.

[25] Y. Lei and T. Li. *Atlas of benthic foraminifera from China Seasthe Bohai Sea and the Yellow Sea*. Berlin, Germany, Springer, 1st edition, 2016.

[26] B. Satyanarayana, M-L Husain, R. Ibrahim, S. Ibrahim, and F. Dahdouh-Guebas. Foraminiferal distribution and association patterns in the mangrove sediments of kapar and matang, west peninsular malaysia. *Journal of Sustainable Science and Management*, 9: 32–48, 2014.

[27] Y.L. Lei, T.G. Li, H. Bi, W.L. Cui, W.P. Song, J.Y. Li, and C.C. Li. Responses of benthic foraminifera to the 2011 oil spill in the bohai sea, pr china. *Marine Pollution Bulletin*, 96(1–2): 245–260, 2015.

[28] V. Stouff, E. Geslin, J.-P Debenay, and M. Lesourd. Origin of morphological abnormalities in ammonia (foraminifera): studies in laboratory and natural environments. *Journal of Foraminiferal Research*, 29(2): 152–170, 1999.

تقييم فعالية التصنيف الخاضع وغير الخاضع للإشراف لصور لاندسات باستخدام تقييم دقة التصنيف

[1,*] حيدر حميد جسوم ، [2] رباب سعدون عبدون

[1,2] قسم الفيزياء،كلية العلوم، جامعة بابل، بابل، العراق.

* **الباحث المسؤول:** *sci685.hadiar.hamied@student.uobabylon.edu.iq*

الخلاصة

في هذه الدراسة تم ملء الفجوات في صور القمر الصناعي لاندسات –7 لعام 2012 باستخدام خوارزمية " معالج أقرب بكسل مشابه " . ومن ثم تم تصنيف وتتبع التغييرات في تغطية استخدام الأراضي / الأغطية الأرضية في محافظة بابل خلال الفترة من 1999 إلى 2023 . حيث تم الاعتماد على صور الأقمار الصناعية لاندسات –7 ولاندسات –8 ، مع التركيز على النطاقات الطيفية المحددة التي توفر دقة مكانية تبلغ 30 مترًا. تم استخدام طريقتي تصنيف: الاحتمال الأقصى للتصنيف الخاضع للإشراف وبيانات ISO للتصنيف غير الخاضع للإشراف. تم استخدام معيار الدقة لتقييم فعالية تقنيات التصنيف الفردية. يتم تحديد هذا المعيار بواسطة نسبة نقاط البيانات المصنفة بشكل صحيح إلى إجمالي حجم مجموعة البيانات. أجرى البحث تحليلاً مقارنا لمنهجيات تصنيف استخدامات الأراضي / الأغطية الأرضية باستخدام صور لاندسات: تصنيف الاحتمال الأقصى الخاضع للإشراف وتصنيف العنقود ISO غير الخاضع للإشراف. أشارت النتائج إلى أن نهج تصنيف الاحتمال الأقصى تفوق أداء طريقة العنقود ISO من حيث الدقة. تم تحديد أربع فئات مميزة لتغطية استخدام الأراضي: الاراضي الحضرية، التربة الجرداء، المسطحات المائية والأراضي الخضراء. حيث كشفت الدراسة عن تغييرات كبيرة في جميع فئات تغطية استخدام الأراضي في محافظة بابل من 1999 إلى 2023 . على وجه الخصوص، أظهرت مساحة الأراضي الحضرية زيادة كبيرة، بينما أظهرت مساحة الأراضي القاحلة انخفاضًا. اختلفت مساحة المسطحات المائية خلال فترة الدراسة، على الأرجح بسبب اختلافات في تصريف المياه من نهر الفرات، الذي يتأثر بالاتفاقيات بين العراق وتركيا وتغيرات هطول الأمطار. كما أظهر توزيع الغطاء النباتي اختلافات سنوية بسبب الخطة التسويقية للجهات المعنية لزراعة المحاصيل الزراعية.

الكلمات الدالة: استخدام الأراضي / الأغطية الأرضية؛ خوارزمية التصنيف؛ التصنيف الخاضع للإشراف؛ التصنيف غير خاضع للإشراف؛ تقييم الدقة.